Trans-scale-scope to find rare cellular activity in sub-million cells

Taro Ichimura,[1,2,*] Taishi Kakizuka,[1] Kazuki Horikawa,[3] Kaoru Seiriki,[4,5] Atsushi Kasai,[4] Hitoshi Hashimoto,[1,4,6,7,8] Katsumasa Fujita,[1,9] Tomonobu M. Watanabe,[10,11] and Takeharu Nagai[1,7,12,*]

[1]Transdimensional Life Imaging Division, Institute for Open and Transdisciplinary Research Initiatives, Osaka University, Yamadaoka 2-1, Suita, Osaka 565-0871, Japan

[2]PRESTO, Japan Science and Technology Agency, Tokyo, 113-0033, Japan

[3] Department of Optical Imaging, Center for Advanced Research Promotion, Tokushima University Graduate School, Kuramoto-cho 3-18-15, Tokushima, Tokushima 770-8503, Japan

[4]Laboratory of Molecular Neuropharmacology, Graduate School of Pharmaceutical Sciences, Osaka University, Yamadaoka 1-6, Suita, Osaka 565-0871, Japan

[5]Institute for Transdisciplinary Graduate Degree Programs, Osaka University, Yamadaoka 1-1, Suita, Osaka 565-0871, Japan.

[6]Molecular Research Center for Children's Mental Development, United Graduate School of Child Development, Osaka University, Kanazawa University, Hamamatsu University School of Medicine, Chiba University and University of Fukui, Yamadaoka 2-2, Suita, Osaka 565-0871, Japan

[7]Division of Bioscience, Institute for Datability Science, Osaka University, Yamadaoka 1-1, Suita, Osaka 565-0871, Japan

[8]Department of Molecular Pharmaceutical Science, Graduate School of Medicine, Osaka University, Yamadaoka 2-2, Suita, Osaka 565-0871, Japan

[9]Department of Applied Physics, Graduate School of Engineering, Osaka University, Yamadaoka 2-1, Suita, Osaka 565-0871, Japan

[10]Laboratory for Comprehensive Bioimaging, RIKEN Center for Biosystems Dynamics Research (BDR), Minatomachi-minami 2-2-3, Chuo-ku, Kobe, Hyogo 650-0047, Japan

[11]Department of Stem Cell Biology, Research Institute for Radiation Biology and Medicine, Hiroshima University, Kasumi 1-2-3, Minami-ku, Hiroshima 734-8553, Japan

[12]The Institute of Scientific and Industrial Research (SANKEN), Osaka University, Mihogaoka 8-1, Ibaraki, Osaka 567-0047, Japan.

*Corresponding authors:

Taro Ichimura, ichimura@otri.osaka-u.ac.jp

Takeharu Nagai, ng1@sanken.osaka-u.ac.jp

Abstract

There are many phenomena in biological systems where less than 1% of rare cells trigger entire multicellular systems. In order to scientifically understand the mechanisms of these rare cell-driven systems, simultaneous observation of huge populations of cells is essential. It has been difficult to observe the dynamics of such phenomena with conventional microscopes. In this study, we propose a novel type of imager, trans-scale-scope, which allows us to observe cell dynamics with sub-cell resolution in a field of view greater than a centimeter. The imaging system is mainly composed of a hundred-megapixel image sensor and a macro-lens for full-size sensor. This method, which is the basement of the future imaging system named AMATERAS (A Multi-scale/modal Analytical Tool for Every Rare Activity in Singularity), realized observation of sub-million cells at the same time. By observing the macroscale-pattern formation process of *Dictyostelium discoideum*, a model organism for studying fundamental aspects of cell-cell communication and chemotaxis, we have shown that the 0.1 % of rare cells triggered a stream of collective cell migration.

Main Text

Introduction

Optical microscopy and cell biology have been mutually heightening over the long history of natural science; Cell biology has taken a new phase by the assistance of innovations in microscopy technology, while microscopy technology has evolved in response to the demands of cell biology.[1] In recent years, one of common directions over both the research communities is simultaneous realization of cell imaging with high spatial resolution and a large field-of-view (FOV) over millimeter scale. If such a microscope is realized, in cell biology, the microscale dynamics at the molecular and single cell level and the macroscale behavior of the entire multicellular system (from tissue to whole body) can be observed simultaneously, and the interaction between the whole system and elements can be understood. The ability to observe a wide FOV at single cell resolution is essential to promote studies on rare cellular activity, as it could allow us to discover rare cells in a large homogeneous cell population, leading to interpretation of their influence to the overall system. This kind of imaging across multiple spatial hierarchy can be termed as "trans-scale imaging", which is important to understand the complex multicellular systems in systems biology, developmental biology and neuroscience. The medical field also has a demand for an imaging system with high spatial resolution and large FOV for quality control in regenerative medicine and for early detection of disease. However, as for microscope optics, since the spatial resolution and magnification are correlated due to the structure of the imaging lens system; a high (low)-resolution imaging system has a high (low) magnification. Due to this fundamental dilemma, expanding the FOV while maintaining cellular resolution has been a difficult task.

In order to expand the FOV with maintaining high spatial resolution in a single imaging system, it is essential to improve both the field number of objective lens and the number of sampling points, that is, pixels on an image-sensor in wide-field imaging and scan points in laser-scan imaging. In recent years, development of fluorescence imaging system for sub-cellular resolution and millimeter FOV has been reported from several groups. One of the cutting-edge technologies was developed by J. Fan *et al.*,[2] which utilizes a custom-made huge objective lens and an array of complementary metal-oxide semiconductor (CMOS) image-sensors to achieve video-rate wide-field (scanless) imaging with lateral spatial resolution of 0.92 μm (at 525 nm) in an FOV of 10 × 12 mm^2. The imaging system, called RUSH (Real-time, Ultra-large-Scale, High-resolution) system, has a great possibility in neuroscience, by which they successfully verified brain-wide-single-cell-resolution imaging of neuronal activities in living mouse. Another type of advanced imaging system was developed by G. McConnell et al.,[3,4] which also uses a custom-made large lens called Mesolens designed for laser-scanning two-photon excited fluorescence imaging, and has achieved three-dimensional imaging with 0.7 μm lateral

resolution in a few millimeters FOV. In addition to neural circuit imaging, whole body imaging of small animals has been realized. The two-photon mesoscope developed by the Janelia Research Campus' group is also a well-established technology using a custom-made objective lens and highly sophisticated illumination technique using the Bessel beam.[5,6]. Rapid volumetric imaging of neuronal activity was realized with synaptic resolution (< 0.6 μm) in a 4.2 × 4.2 × 0.1 mm^3 volume. Many other techniques have been proposed to show the possibility of expansion of the FOV with cellular resolution with mainly targeting the application to neuroscience.[7,8,9,10]

In the studies described above, a specially designed large lens is one of the key components in both the wide-field imaging[2] and laser-scan imaging.[3,4,5,6] As long as classical lens-imaging system is employed, a larger size of lens beyond the conventional ones is essential to achieve the trans-scale imaging. However, these objective lenses are one-and-only ones made with high technology and high cost, making it difficult to disseminate them widely in the large research communities of biology and medicine. Also, while these have been made to high-end specifications mainly for applications to neuroscience and developmental biology, many other biological and medical studies require inexpensive and easy-to-use devices with somewhat moderate performance. The same argument applies to detection methods. In other words, fast scanning and beam shaping of image sensor arrays and pulsed lasers are beyond the reach of the general biologist in terms of both technology and cost. The availability of simpler, easier-to-use detection options is important for opening up new areas in biology and medicine.

In this paper, we propose a versatile configuration for trans-scale imaging with an over-one-centimeter FOV and sub-cell resolution using a hundred-megapixel image-sensor, which we named AMATERAS (A Multi-scale/modal Analytical Tool for Every Rare Activity in Singularity). We aim to eventually establish AMATERAS as a multimodal measurement instrument, but the current version (AMATERAS1.0) possesses only a single modality (optical microscopy). In the recent biology, wide-field fluorescence microscopes employ either electron-magnifying charge-coupled device (EM-CCD) or scientific CMOS (sCMOS) sensors, and accordingly can achieve ultra-high sensitivity down to single-photon level. However, the number of pixels of a single image sensor is typically smaller than 10 megapixels on the market. In contrast, sensors developed for machine vision have a wider variety of options with much more pixels. Here, we propose a strategy of construction of a fluorescence imaging system using a 120 megapixel CMOS image sensor (120MXSM) developed by CANON Inc., which is one of the largest commercially available image-sensors. The CMOS chip has 13264 × 9180 effective pixels with 2.2 μm pixel size and 29.2 mm × 20.2 mm chip size (APS-H). Because of the small pixel size, a magnification of imaging system around 1x is sufficient when a given research requires spatial resolution at the single-cell level. Imaging lenses for APS-H

sensor sizes at such magnifications are not present in the lineup of biological microscope objectives, but are available in those for machine vision applications. Here, we selected a 2x imaging lens (LSTL20H-F, Myutron, Japan) because of its relatively high numerical aperture (*NA* = 0.12) as well as a large field-number (44 mm). The combination of the above image sensor and the imaging lens allows for imaging of an FOV of 14.6 × 10.1 mm^2 (17.8 mm diagonal) with a spatial resolution better than 2.5 μm in the visible wavelength region. Our read-out system employing the high speed CoaXpress interface allows for the maximum speed of 9.4 frame per second, which corresponds to the data throughput of 1.14 gigapixels per second.

The wide-field imaging configuration using a single CMOS chip has the advantage that the entire FOV can be recorded almost simultaneously without leaking information. This is beneficial for live cell observation, especially searching for rare cells and tracking individual cells. In the following sections, we first evaluate the optical performance and biological applicability by some fundamental measurement of fluorescent beads and fixed specimens, and demonstrate a possibility of time-lapse imaging of collective cell migration using cultured epithelial cells. We then show the application of the method to a study of rare cellular activity. We chose *Dictyostelium discoideum* (*D. discoideum*) as a model system, and realized the time-lapse imaging of their chemotaxis and macroscopic pattern formation in the over-one-centimeter FOV. In Discussion, we compare our AMATERAS system with the conventional imaging system and the previous reports from other groups, and finally discuss the necessity and possibility of the improvement of the optical performance for the future applications.

Results

Configuration and performance of over-one-centimeter-FOV imaging system

Figure 1a shows the schematic configuration of the AMATERAS1.0 system. An inverted microscope configuration was employed for imaging cultured cells. A camera equipped with the 120-megapixel CMOS sensor (VCC-120CXP1M, CIS, Tokyo, Japan) was used. The imaging lens was directly connected with the camera through the F-mount. High-brightness LEDs with different three colors (Thorlabs, New Jersey) were equipped for fluorescence excitation. Because of the long working distance of the imaging lens (~110 mm), the fluorescence excitation light was illuminated obliquely from the bottom of the sample. Bright-field imaging was done with another white-light LED placed at the top of the sample. All the LEDs were switched on/off under computer control. Details of the optical devices and components are described in the Materials and Methods section and the detailed configuration is found in the supplementary Fig. S1.

To demonstrate the imaging performance, fixed Madin-Darby Canine Kidney (MDCK) epithelial cells were observed both in the bright-field transmission mode and in the fluorescence mode. The nuclei of the cells were stained with a nucleus-staining green fluorescent chemical probe, NucleoSeeing (Funakoshi, Tokyo, Japan).[11] The LED with a center wavelength of 470 nm was used, and the green fluorescence centered at 520 nm was detected. The image-set in Fig. 1b certificated that the individual single cells could be clearly resolved separately over the full FOV with 14.6 × 10.1 mm^2 square. Since the cells were cultured until the confluent state, we were able to estimate the maximum number of cells in the FOV by counting the number of nuclei. The number of cells was found to be about 227,000 in this case, which is much larger than normal microscopes.

For evaluation of the spatial resolution, we performed imaging of fluorescent beads with 200 nm diameters to experimentally record a point spread function (PSF) of the imaging system. The LED with a center wavelength of 470 nm was used, and the green fluorescence from the beads with center wavelength of 520 nm was detected. Figure 1c shows representative images of the 200 nm beads in transverse (*xy*) and longitudinal (*yz*) planes at the center and corner of the FOV. The *yz* plane image is a longitudinal cross-section of an image-stack obtained by scanning the sample-lens distance in the *z* direction. The lateral spatial resolution and axial depth of focus were estimated by full-width of half-maximum (FWHM) of Gaussian fit to the bright spot. Figure 1d-e show line profiles along (d) the *y* axis at the in-focus plane and (e) the *z* axis penetrating the center of the bright spots. The FWHM of the bright spot in the transverse plane was found to be 2.25 μm and 2.28 μm at the center and corner, respectively. This difference does not have statistical significance, as the *t*-test of 50 samples (50 bright spots for each) did not significantly reject the null hypothesis ($p = 0.24$). The experimental FWHMs were found close to the theoretical value, 2.17 μm, which was calculated by FWHM of theoretical PSF ($\sim 0.51\lambda/NA$) for $NA = 0.12$ and $\lambda = 520$ nm.[12] As for the *z*-direction (Fig. 1e), because of the low NA (= 0.12), the depth of focus was found to be much longer than the transverse plane, 62.4 μm at the center and 69.4 μm at the corner. The difference between the center and corner (Fig. 1e) was not statistically significant, either, according to the *t*-test for 50 samples ($p = 0.85$). The mean value of FWHM, 64.0 μm at the center, was close to a numerically calculated one, 60.6 μm, based on scalar integration of converging plane waves (Fig. S2a-b). The numerical calculation also guaranteed that the spherical aberration due to the presence of glass plates (170-μm-thick cover glass of the sample dish and a 2-mm-thick glass of the emission filter) is almost negligible (Fig. S2b-c). These results indicate that the theoretically expected resolution is realized without aberration over the entire FOV, and special care for non-uniformity of spatial resolution will not be necessary.

We compared the lens and camera used in the AMATERAS1.0 system with lens system and sCMOS camera which are generally used in recent cell biology. The results are shown as supplementary data (Fig. S3), where the larger FOV (Fig. S3a and b) and the finer sampling (Fig. S3a and c) is achieved than the conventional microscope configuration. Through these evaluations, the imaging system proposed in this study has been proven superior to conventional imaging systems in terms of FOV and spatial resolution.

Multi-color imaging of mouse brain slice

The AMATERAS1.0 system is capable of multi-color fluorescence imaging, which is indispensable for understanding of biological systems with multiple feature parameters (proteins, cations, membranes, etc.) in the modern cell biology. Multi-color imaging can be done with sequentially switching the combination of LEDs, excitation filters, and emission filters among three wavelength bands. As a demonstration of multi-color imaging, we performed trans-scale imaging of a centimeter-wide mouse brain section. A fixed mouse brain slice was prepared with a protocol described in Materials and Methods. The two types of fluorescent proteins, tdTomato [13] and EGFP, were expressed in excitatory projection neurons and inhibitory interneurons, respectively. In addition, the nuclei of all the cells were stained with Hoechst 33342. Figure 2a shows a trans-scale multi-color image of a 25-μm-thick slice, which is an RGB image reflecting the fluorescence intensities of tdTomato (red), EGFP (green), and Hoechst (blue). The left panel exhibits the full FOV, where the whole brain scale is covered in the single FOV, so that only a few seconds is required to acquire the three images for the three wavelength bands. Any specific region can be zoomed in to see a local distribution of the cells at single cell resolution. For instance, two regions of the brains indicated with the light-blue squares (*A*: cerebral cortex, *B*: hippocampus) are magnified by 5-fold, as shown in the middle top and bottom panels. The light-blue square region in the 5x images are further magnified by 5-fold in the right panels, where distribution of single neuronal cells is clearly recognized.

In the recent neuroscience, whole brain imaging is a hot topic. Combination of tissue clearing and light-sheet microscopy technology realized all neuron imaging in a whole mouse brain.[14,15] We had also proposed another type of whole brain imaging technique, block-face serial microscopy tomography (FAST).[16,17] In the methods used in the above reports, images obtained with a smaller FOV are tiled to cover the whole size of a brain c.a. 1 cm cube, which takes a few minutes to a few tens of minutes for a single section, and accordingly the three-dimensional imaging of a whole brain requires many hours. In contrast, our AMATERAS1.0 is capable of imaging an over-one-centimeter size in a single shot, holding a potential to drastically reduce the total imaging time.

Time lapse imaging of collective cell migration

The ability to observe a large number of cells in the large FOV is advantageous in investigation of the mechanism of multi-cellular systems dynamics. One can directly find and observe the impact of rare cells and local phenomena occurring in macro-scale dynamics. Here, we demonstrate the effectiveness of our imaging system in collective cell migration, which is an important object in cell biology. Collective migration is involved in various functions in living systems,[18] and there have been many studies on signaling mechanisms and leader-follower interactions.[19,20] We set our imaging target to the wound healing phenomenon of MDCK epithelial cells. The wound healing is a well-studied cellular function, which can be observed when cultured epithelial cells in the confluent state is partially stripped. We used MDCK cells expressing EGFP at a membrane protein (See Materials and Methods). They were cultured in a glass-bottom dish to confluence, and image acquisition was started 20 hours after stripping and was repeated at the 10 minutes interval until 24 hours passed since the beginning of the acquisition. The 24-hour video of the full FOV can be found as supplemental material (Movie 1). Figure 3b shows the fluorescence images of the first and last frames of the full FOV. The cells on the left half of the FOV were stripped, and the "wound" was being healed. An enlarged view within the images emphasize that each cell can be obviously identified individually. The number of cells in the FOV in the confluent state before stripping was estimated to be about 700,000. Comparing the last frame (bottom) with the first frame (top), we can see that the edge of the cells has been extended by approximately 500 μm because of the collective migration. Figure 3c-d show the seven frames at the interval of 4 hours in the two regions indicated by the light-blue squares near the edge (*A*) and an area away from the edge (*B*) in Fig. 3b. In Fig. 3c, cell migration and deformation of individual cells can be tracked at a single cell level within the dynamic change of the multi-cellular system (See Movie 2). In more detail, the cells in the 1 mm vicinity of the migration frontline are actively dividing and moving, while no collective movement was observed at the cells far from the frontline as shown in the right side of Fig. 3d.

Finding rare cellular activity in macroscale pattern formation of *D. discoideum*

In order to show the applicability to the system biology, trans-scale imaging of macroscale pattern formation of *D. discoideum* was performed. It is well known that *D. discoideum* cells, when starved, interact each other by means of cyclic-adenosine-monophosphate (cAMP) concentration waves as a signal, self-assembles spiral and concentric waves over a centimeter range, and eventually form aggregates into a slug form.[21] There have been a plenty of studies aimed at elucidating the mechanism leading to this pattern formation [22,23,24] There are multiple hypotheses on the mechanism and it is still controversial.[25,26,27] However, in the previous studies, either imaging with a wide FOV and low-resolution or that with a narrow FOV and high-resolution has been independently employed, which makes it difficult to conduct the elucidation studies by direct observation.

Here, we suggest that our AMATERAS1.0 system can contribute to this subject, as it can realize simultaneous imaging of single cell signaling and global pattern formation, for the first time. To visualize the cAMP concentration, we used *D. discoideum* cells expressing fluorescent reporter, a fusion protein of Flamindo2 [28] and mRFP, [29] which are respectively sensitive and insensitive to the cAMP concentration. Flamindo2 is an OFF-type yellow fluorescent indicator for cAMP. Ratiometric imaging of the two color-channels allowed for visualization of cAMP concentration distribution. Images were recorded every 30 seconds in 15 hours since 3 hours after the cells were starved ($t = 0$). See Materials and Methods for details of the sample preparation and measurement scheme.

Figure 3 shows a part of image dataset at characteristic time ranges. Figure 3a shows a time evolution of macroscopic pattern over a long-time scale. The number of cells observed in the FOV was approximately 130,000 cells. There was no clear generation of macroscopic pattern until seven hours after the starvation (left panel). About nine hours after the starvation treatment (second-left), it was clearly seen that cAMP concentration waves were repeatedly generated and propagated. As time goes on, the spatial pattern of the wave of cAMP concentration changed to concentric wave (second-right), and eventually the cells migrated toward the centers of the concentric circle (right) to form multicellular aggregates. Overall movies of the full FOV with reduced resolution is found as a supplementary material (Movies 3).

In the early stage (t = 6h40m0s, Fig. 3a left), the macroscopic pattern had not been seen. However, we can find rare cells with high cAMP concentration which may work as a trigger of the subsequent pattern in the macroscale. Figure 3b shows successive four frames at one-minute intervals (every other frame) of the closeup of the white square in the left panel of Fig. 3a. The spatial resolution of the imaging is high enough to recognize single cell morphology. In the closeup views, only a few cells among more than hundred cells impulsively exhibited prominent cAMP concentration. It seems that the cell pointed by a white arrow is the leader and the other cells pointed with the pink and light-blue arrows are followers which have already been excitable triggered by the leader. A movie file of this local region is found as a supplementary material (Movies 4). This leader cell was found to be almost the first emerging leader cell among the 130,000 cells. More detailed analysis of the big dataset allows investigation of the mechanism of the macroscale pattern formation generation triggered by the rare leader-cells. We have intensively performed such a systems-biological analysis and discussion, and revealed that only 0.13 % of cells work as pace-making cells to lead their surrounding cells to eventually form a large-scale spiral wave of cAMP concentration. The detail of the discussion is described elsewhere.[30]

In the subsequent time range, triggered by the leader cells, more cells started to generate the cAMP pulse, and synchronously generated a macroscale wave over the centimeter scale. Figure 3c shows successive four frames at one-minute intervals of the macroscopic views (top) and closeup views (bottom) of the square region in the top left panel of Fig. 3c. In this phase, all cells undergo pulsing of cAMP and act as carriers for propagating waves, forming a spiral wave pattern throughout the FOV. The next phase of the macroscale pattern was seen around t = 15h10m0s (second right panel in Fig. 1a). Figure 3d shows successive four frames at one-minute intervals of the macroscopic views (top) and closeup views (bottom) of the local region surrounding a center of concentric wave indicated with the white square in the top left panel of Fig. 3d. While concentric waves are propagating outward in the macroscopic views, it can also be seen that individual cells are migrating toward the center of the concentric circle.

Discussion

In this paper, we proposed an imaging system for sub-cell resolution in over-one-centimeter FOV using a hundred-megapixel image-sensor and camera lens designed for machine vision purpose. Fluorescence imaging of living cells has been shown with a single-cell resolution in a much larger FOV than conventional biological microscopes. For visual comparison of spatial resolution and FOV, our AMATERAS1.0 system and several conventional imaging systems (combinations of imaging lens and image sensor) were plotted on Fig. 4, with the vertical axis representing spatial resolution and the horizontal axis representing FOV size (diagonal). We selected five series of objective lens of three microscope companies (Olympus, NIKON, Thorlabs), and two widely used image sensors of Andor. See the figure legend for detail.

Here, the effective spatial resolution (d) is defined as the larger one of two types of spatial resolution limit based on optical diffraction (d_{lens}) and pixelation at image sensor (d_{sensor}).

$$d = \max(d_{lens}, d_{sensor}) = \max\left(C\frac{\lambda}{NA}, 2a\right) \quad (1)$$

Here, λ and a denotes wavelength of light and pixel size of image sensor, respectively. The coefficient C depends on resolution criterion (0.5 for Abbe's criterion, 0.61 for Rayleigh's criterion, 0.47 for Sparrow's criterion), but here the Abbe's criterion (C = 0.5) should be adopted to compare with the sampling rate by the pixelation. On the other hand, the FOV size (Φ) is defined as the smaller one of FOVs restricted by lens system (Φ_{lens}) and image sensor (Φ_{sensor}).

$$\Phi = \min(\Phi_{lens}, \Phi_{sensor}) = \min\left(\frac{FN}{M}, \frac{\phi}{M}\right) \quad (2),$$

where FN, ϕ, and M denote the field number of lens system, physical size of the image sensor, and the magnification of the lens system. To represent the ability of covering the

scale hierarchies, we introduce "trans-scalability index", r, which we defined by the ratio of one-dimensional FOV (Eq. 2) to lateral spatial resolution (Eq. 1) as

$$r = {\Phi}/{d} \tag{3}$$

This index has the same function with the space-bandwidth product proposed in previous literature,[31] but offers more intuitive understanding of scale hierarchy covered by the optical system. In other words, the index represents the number of effective sampling points at which the full FOV is divided on its diameter. Contour lines of the trans-scalability index are drawn in Fig. 4.

To achieve a high trans-scalability index (r) in the wide-field imaging, having a large number of pixels is the minimum requirement. At the same time, the chip size must be within the FOV of the lens system, and as a result, a small pixel size is also a requirement. The maximum value for a given image sensor is achieved when the chip size is less than the FOV of the lens system and the pixel size is greater than half of the optical resolution ($d_{\mathrm{sensor}} > d_{\mathrm{lens}}$). For low-magnification ($M < 10$) lenses, this condition is largely met, so the markers in the plot of Fig. 4 are aligned along image sensor-dependent contours ($r_{\mathrm{max}} = \Phi_{\mathrm{sensor}}/d_{\mathrm{sensor}}$). The two types of scientific cameras, Zyla 5.5 and iXon Ultra 888 (Andor, Belfast, UK), have chip sizes of 21.8 mm and 18.8 mm, and pixels of 6.5 μm and 13 μm, respectively, so the maximum values of r are $r_{\mathrm{max}} = 1677$ and $r_{\mathrm{max}} = 723$, respectively. This limit cannot be exceeded with any lens system. On the other hand, in the high magnification region ($M > 10$), there is often oversampling ($d_{\mathrm{sensor}} < d_{\mathrm{lens}}$) and the value of r decreases. Compared to these conventional cases, in this present study, a sensor with an extremely high number of pixels was used, which results in an r value of 7487. Since the lens system was selected so that the spatial resolutions due to the lens system and image sensor are comparable ($d_{\mathrm{sensor}} \sim d_{\mathrm{lens}}$), it can be said that this is an ideal configuration that achieves a high r without compromising the optical resolution at the sub-cellular scale.

Imaging systems reported by other groups[2,4,6] are also plotted in Fig. 4 for comparison. The values of spatial resolution and FOV reported in the paper were adopted for the plots, even though the performance is still being improved. Our AMATERAS1.0 system outperforms the other groups with respect to the FOV, as it prioritizes the expansion of the lateral FOV over resolution. On the other hand, the AMATERAS1.0 system is inferior in terms of spatial resolution due to the low NA of the imaging lens. Our advantage is that this performance can be realized with relatively low-cost devices, which has wide application possibilities.

In this paper, we demonstrated that our method is effective in imaging multicellular systems formed by a large number of cells in different epigenetic states and in measuring

their temporal dynamics. This method can easily obtain necessary information when examining the heterogeneity or the effect of rare cells within a huge population. Although not demonstrated in this paper, we believe that it is a promising method for studying heterogeneity in cell differentiation. In a previous literature,[32] the heterogeneity was investigated based on statistical analysis of imaging data of more than thirty thousand of cells, which however was a time-consuming work. Rapid data acquisition is desirable to circumvent the possibility of questioning the consistency of the experimental environment. Our method can measure more than hundred thousand cells in the same time on a single FOV, and can also obtain time series data. Thus, it has the potential to provide useful data for research in this area.

Another important direction of application is to speed up tissue biopsy. In recent years, the automation of tissue biopsy using the artificial intelligence (AI) has been proposed and studied worldwide for practical use. Faster data acquisition is an important technical challenge, both in the collection of supervisory data and in the actual diagnosis of a large number of specimens. A variety of medical instruments manufacturers have marketed high-speed image acquisition systems with automatic scanning mechanisms. The imaging system in this paper can also observe a much larger area with cellular resolution than conventional microscopes in a single shot, allowing rapid observation of large sections in a single shot. In addition, it will be possible to design a device that observes a large number of sections in parallel and simultaneously. Thus, it has great potential to contribute to the field of medical diagnosis.

Since the present imaging system is a wide-field (scanless) imaging system, it is not capable of depth discrimination. It is intended for imaging of two-dimensional culture systems and sections. In order to obtain depth resolution, it is necessary to introduce a confocal scanning type or a multi-photon excitation type. By using a mechanism for selectively illuminating a specific plane on the illumination side, three-dimensional imaging can be realized. For example, introductions of light sheet illumination and spatiotemporal focusing are realistic candidates. Near-surface imaging using total reflection illumination is also one option.

Conclusion

In conclusion, we have proposed a trans-scale imaging system, the AMATERAS1.0 system, that enables live-cell imaging within a FOV of 17.8 mm diagonal. Imaging with fluorescent beads showed that a spatial resolution of 2.2 μm could be obtained over the entire FOV. The imaging of nucleus-stained fixed cells and membrane-stained live cells showed that the method can be used to study cell biology and developmental biology. The imaging system has been successfully applied to imaging of pattern formation of *D. discoideum* cells and finding rare leader-cells among more than hundred thousand cells,

which certificated that our method can be applied to the study of system biology. This research is still a starting point, and we would like to develop it into an imaging technology with a wider FOV, higher resolution, and three-dimensional resolution.

Acknowledgements

This work was supported by a Grant-in-Aid for Scientific Research on Innovative Areas “Singularity Biology (No.8007)” (18H05415 to KH, 18H05416 to HH and 18H05408 to TN), the Research Program of "Five-star Alliance" in "NJRC Mater. & Dev." (KH, TN), and Precursory Research for Embryonic Science and Technology (PRESTO) of Japan Science and Technology Agency (JST) (TI). We thank Y. Yoshihara, J. Kajiwara, K. Morimoto, and other members of the KH’s laboratory for technical assistance. We also acknowledge the Dicty Stock Center for providing us the pDM304, pDM358, and Ax2 cell lines.

Materials and Methods

Imaging system: AMATERAS1.0

The imaging system (**AMATERAS1.0,** Fig. 1a, Fig. S1) was built using DIY components served from Thorlabs and OptSigma. We used a vertical support rail (CEA1600, Thorlabs, New Jersey) as a main microscope body. An inverted microscope configuration was employed for imaging cultured cells. A camera (VCC-120CXP1M, CIS, Tokyo, Japan) equipped with the 120-megapixel image-sensor (120MXSM, Canon, Japan) was used. The imaging lens uses a machine vision lens (LSTL20H-F, Myutron, Tokyo, Japan). Due to its long working distance, the fluorescent excitation light is illuminated obliquely from below the sample, which allows for epi-fluorescence imaging without a dichroic mirror. The excitation light uses three-color high-intensity LEDs centered at wavelengths of 525 nm, 470 nm, and 385 nm (SOLIS-525C, SOLIS-470C and SOLIS-385C, Thorlabs, New Jersey), for which we used three sets of excitation filters (#86-963, #86-962, #33-322, Edmund Optics, New Jersey) and fluorescence filters (#67-048, #86-366, #84-111, Edmund Optics, New Jersey) with 2 inch diameters. The excitation filters are placed just after the LEDs. The LED emissions are combined at two dichroic beam-combiners (#86-399, #86-396, Edmund Optics, New Jersey) into the same path. The light is relayed by a lens system with 0.5x magnification composed of two lenses, L1 (f = 150 mm, LA1417-A-ML, Thorlabs, Japan) and L2 (f = 75 mm, LA1145-A-ML, Thorlabs, Japan), and reflected up by a mirror toward the bottom surface of the sample. The incident angle is around 20 degree, which was chosen to be larger than arcsine of the NA of the imaging system (= 0.12) to avoid the direct reflection from striking into the imaging lens. The LEDs were switched on/off by a trigger signal from a computer through a DAQ board (NI USB-6001, National Instruments, Austin, Texas). The fluorescence filters were switched by a motorized wheel for 2-inch filter (#59-769, Edmund Optics, New Jersey). However, only for the imaging of *D. discoideum* cells, the two fluorescence filters (#67-048, #86-366) were switched by a filter flip mount (MFF102/M, Thorlabs, New Jersey) for high speed switching. To control the focus position, the lens and camera were mounted on a single translation stage (PT1/M, Thorlabs, New Jersey) with a motorized actuator (SOM-C25E, OptoSigma, Tokyo, Japan), and the entire stage was moved up and down in adjusting the focus position. A stage-top incubator (U-140A, BLAST, Kawasaki, Japan) was used for the sample stage to control the temperature and CO_2 concentration. The position and angle of the sample stage were adjusted by a five-axis manual stage composed of three translation stages (TSD-651C25-M6, TSD-651C-M6, TASB-653-M6, OptoSigma, Tokyo, Japan), and two goniometer stages (GOHT-65A50BMS-M6 and GOHT-65A75BMSR-M6, OptoSigma, Tokyo, Japan). In particular, fine angle-adjustment by the goniometer stages was indispensable for the imaging in the wide FOV. The angle was adjusted so that the height difference was within the depth of focus at each end of the FOV. The stage, lens and camera were housed in a dark box to block out the background light and to suppress the influence from ambient temperature fluctuation.

Preparation of mouse brain slice

Male C57BL/6J mice at 7-week-age were purchased from SLC (Shizuoka, Japan) and used for experiments at least 1 week after animal transportation. Mice were maintained with group housing (usually n = 3–6 per cage) on a 12-h light-dark cycle (lights on at 8:00 a.m.) at a controlled room temperature. Water and food (CMF, Oriental Yeast, Osaka, Japan) were available *ad libitum*. All animal care and handling procedures in mice were approved by the Animal Care and Use Committee of Osaka University. All efforts were made to minimize the number of animals used.

For viral construct, pAAV-mDlx-GFP-Fishell-1 was kindly provided by Gordon Fishell (Addgene plasmid #83900; http://n2t.net/addgene:83900; RRID: Addgene_83900) (Dimidschstein et al., Nat Neurosci, 2016). The AAV plasmid vector including the mouse alpha-CaMKII promoter was kindly provided by Akihiro Yamanaka (Nagoya University), and pAAV-CaMKII-tdTomato-WPRE was constructed by insertion of the tdTomato open reading frame.

AAV packaging and titration was performed as previously described (Challis et al., Nat Protoc, 2019) with minor modifications. Briefly, AAV transgenes were packaged using an AAV helper-free packaging system (catalog no. VPK-400-DJ; Cell Biolabs, San Diego, CA) except for the plasmid carrying AAV rep and cap genes. A plasmid vector carrying the AAV PHP.eB capsid was synthesized by Ken-ichi Inoue (Kyoto University) and Masahiko Takada (Kyoto University) according to the original paper of the PHP.eB capsid (Chan et al., Nat Neurosci, 2017). The AAV transgene plasmid, AAV helper plasmid and AAV rep and cap plasmid for the PHP.eB capsid were co-transfected into HEK293T cells using polyethyleneimine (catalog no. 24765; Polyscience, Inc., Warrington, PA). The cells and culture media were separately harvested after 72 h after transfection, and crude AAV preparation was obtained by freeze-thaw cycle of the cell suspension in the lysis buffer (10 mM Tris, 10 mM $MgCl_2$ and 150 mM NaCl, pH 7.6) and polyethylene glycol precipitation from the culture media. Crude AAV preparation was treated with ≥250 units/μL Benzonase® Nuclease (catalog no. E1014; Sigma-Aldrich, St Louis, MO), and the supernatant was collected after centrifugation at 3,000 × g for 15 min at room temperature. Viral vectors were purified by iodixanol (Optiprep, catalog no. AXS-1114542; Cosmo Bio Co., Tokyo, Japan) density gradient ultracentrifugation.

The viral titers were determined by quantitative real-time PCR using GoTaq® qPCR Master Mix (Promega, Madison, WI) on a CFX96 Touch™ Real-Time PCR Detection System (Bio-Rad, Hercules, CA) with a linearized pAAV-mDlx-GFP-Fishell-1 as a standard.

Viral injection and tissue preparation

Mice were intravenously injected with a viral cocktail including AAV-PHP.eB-CaMKII-tdTomato-WPRE and AAV-PHP.eB-mDLX-GFP at $1\times10_{11}$ viral genomes/virus. Three weeks after viral injection, mice were deeply anesthetized by intraperitoneal injection of the anesthetic cocktail at a dose of 4 mg/kg midazolam (Dormicum, Astellas, Tokyo, Japan), 0.3 mg/kg medetomidine (Domitor, ZENOAQ, Fukushima, Japan) and 5 mg/kg butorphanol tartrate (Vetorphale, Meiji Seika Pharma, Tokyo, Japan), and were transcardially perfused with 10 ml saline followed by 15 ml 4% paraformaldehyde dissolved in phosphate-buffered saline (PBS). Brain tissues were excised and stored in 4% paraformaldehyde dissolved in PBS at 4 °C overnight and transferred in 0.05% sodium azide dissolved in PBS.

Tissue sections were prepared at 25-μm-thickness using a vibrating microslicer (LinearSlicer Pro7N, Dosaka EM, Kyoto, Japan). After nuclear staining in 1 μg/ml Hoechst 33258 dissolved in PBS, tissue sections were mounted on glass slides and coverslipped with ProLong Glass antifade mountant (catalog no. P36982, Thermo Fisher, Waltham, MA).

Preparation and imaging for MDCK cells

The MDCK CIBN-pmGFP cells were cultured on 35mm grass bottom dish (AGC Techno Glass, Shizuoka, Japan) until confluent at 37₀C with 5% CO2 in D-MEM (043-30085, Wako, Osaka, Japan) supplemented with 10% FBS (FB-1365, Biosera, France) and 100 units/ml penicillin and 100 μg/ml streptomycin (168-23191, Wako, Osaka, Japan). For nuclei observation, cells were fixed with 4% paraformaldehyde for 10 min, washed by PBS, permeabilized with 0.2% Triton X-100 for 10 min, washed by PBS aging, and then stained with 5μM NucleoSeeing (Funakoshi, Tokyo, Japan) in PBS. Images were obtained using the AMATERAS1.0 system with excitation by 470nm LED. For live imaging of wound healing, a wound was created at t=0h by peeling off a part of the confluent cells using cell scraper (ASONE, Osaka, Japan). Then, the dish was put on the stage top incubator which kept at 37₀C with 5% CO_2, and wound healing process was imaged by the AMATERAS1.0 system for 24 hours from t=20h to t=44h with 10 minutes frame interval. The intensity and exposure time of the excitation light (LED, 470 nm) were 26.9 mW/cm2 at the sample plane and 5 seconds, respectively.

Preparation and imaging of *D. discoideum*

The Ax2 is routinely maintained on a 9 mm plastic dish at 22₀C in HL5 medium[33] supplemented with 50 μg/ml hygromycin (Wako, Osaka, Japan) and 16 μg/ml G418 (Wako, Osaka, Japan). Cultured cells were suspended by pipetting on the dish and split into new dish at about 1:6 ratio every 24 hours, which cells were maintained almost

constant cell number for long time. Development of the cells were started at t=0h by inducing starvation as washed gently three times, so as not to be peeled off from the dish surface, by development buffer (5 mM Na2HPO4, 5 mM KH2PO4, 1 mM CaCl2, 2 mM MgCl2, pH 6.4). Then, these cells were suspended in the developmental buffer and the cell number was counted by using Countess-II (Thermo Fisher Scientific, Massachusetts, USA). 1.0 x 10_6 cells were plated on a 35mm glass bottom dish (AGC Techno Glass, Shizuoka, Japan) in 1.6 ml of developmental buffer. The dish was put on a stage chamber at 22_oC and imaged by the AMATERAS1.0 system for 15 hours from t=3h to t=18h. Imaging interval of time-frames was 30 sec, resulted in 1,800 time-frames for 15 hours observation. At each time frame, fluorescence of Flamindo2 and RFP were sequentially imaged. The excitation intensity of the two LEDs was 2.8 mW/cm_2 (470 nm) and 5.0 mW/cm_2 (525 nm) at the sample plane, respectively. Both fluorescence was detected with 2 sec exposure with x8 gain.

References

1 Milestones in light microscopy. Nature Cell Biology 11, 1165 (2009).
2 Fan, J. et al. Video-rate imaging of biological dynamics at centimetre scale and micrometre resolution. Nat. Photonics (2019). doi:10.1038/s41566-019-0474-7
3 McConnell, G. et al. A novel optical microscope for imaging large embryos and tissue volumes with sub-cellular resolution throughout. Elife 5, (2016).
4 McConnell, G. & Amos, W. B. Application of the Mesolens for subcellular resolution imaging of intact larval and whole adult Drosophila. J. Microsc. 270, 252–258 (2018).
5 Sofroniew, N. J., Flickinger, D., King, J. & Svoboda, K. A large field of view two-photon mesoscope with subcellular resolution for in vivo imaging. Elife 5, (2016).
6 Lu, R. et al. Rapid mesoscale volumetric imaging of neural activity with synaptic resolution. Nat. Methods 17, 291–294 (2020).
7 Terada, S.-I., Kobayashi, K., Ohkura, M., Nakai, J. & Matsuzaki, M. Super-wide-field two-photon imaging with a micro-optical device moving in post-objective space. Nat. Commun. 9, 3550 (2018).
8 Yoshida, E. et al. In vivo wide-field calcium imaging of mouse thalamocortical synapses with an 8 K ultra-high-definition camera. Sci. Rep. 8, 8324 (2018).
9 Werley, C. A., Chien, M.-P. & Cohen, A. E. Ultrawidefield microscope for high-speed fluorescence imaging and targeted optogenetic stimulation. Biomed. Opt. Express 8, 5794 (2017).
10 Park, J. H., Kong, L., Zhou, Y. & Cui, M. Large-field-of-view imaging by multi-pupil adaptive optics. Nat. Methods 14, 581–583 (2017).
11 Nakamura, A. et al. Hoechst tagging: A modular strategy to design synthetic fluorescent probes for live-cell nucleus imaging. Chem. Commun. 50, 6149–6152 (2014).
12 Udo J. Birk, Super-Resolution Microscopy: A Practical Guide, Wiley-VCH (2017/12/4).
13 Shaner, N. C. et al. Improved monomeric red, orange and yellow fluorescent proteins derived from Discosoma sp. red fluorescent protein. Nat. Biotechnol. 22, 1567–1572 (2004).
14 Susaki, E. A. et al. Whole-brain imaging with single-cell resolution using chemical cocktails and computational analysis. Cell 157, 726–739 (2014).
15 Ueda, H. R. et al. Whole-Brain Profiling of Cells and Circuits in Mammals by Tissue Clearing and Light-Sheet Microscopy. Neuron 106, 369–387 (2020).Susaki, E. A. et al. Whole-brain imaging with single-cell resolution using chemical cocktails and computational analysis. Cell 157, 726–739 (2014).
16 Seiriki, K. et al. High-Speed and Scalable Whole-Brain Imaging in Rodents and Primates. Neuron 94, 1085–1100 (2017).
17 Seiriki, K. et al. Whole-brain block-face serial microscopy tomography at subcellular resolution using FAST. Nat. Protoc. 14, 1509–1529 (2019).
18 Friedl, P. & Gilmour, D. Collective cell migration in morphogenesis, regeneration and cancer. Nature Reviews Molecular Cell Biology 10, 445–457 (2009).
19 Farooqui, R. & Fenteany, G. Multiple rows of cells behind an epithelial wound edge extend cryptic lamellipodia to collectively drive cell-sheet movement. J. Cell Sci. 118,

51–63 (2005).
20 Yamaguchi, N., Mizutani, T., Kawabata, K. & Haga, H. Leader cells regulate collective cell migration via Rac activation in the downstream signaling of integrin β1 and PI3K. Sci. Rep. 5, 1–8 (2015).
21 Kessin, R. H. Dictyostelium: evolution, cell biology, and the development of multicellularity, vol. 38 (Cambridge University Press, 2001).
22 Gregor, T., Fujimoto, K., Masaki, N. & Sawai, S. The onset of collective behavior in social amoebae. Science (80-.). 328, 1021–1025 (2010).
23 Sawai, S., Thomason, P. A. & Cox, E. C. An autoregulatory circuit for long-range self-organization in Dictyostelium cell populations. Nature 433, 323–326 (2005).
24 Lee, K. J., Cox, E. C. & Goldstein, R. E. Competing patterns of signaling activity in dictyostelium discoideum. Phys. Rev. Lett. 76, 1174–1177 (1996).
25 Levine, H., Aranson, I., Tsimring, L. & Truong, T. V. Positive genetic feedback governs cAMP spiral wave formation in Dictyostelium. Proc. Natl. Acad. Sci. U. S. A. 93, 6382–6386 (1996).
26 Lauzeral, J., Halloy, J. & Goldbeter, A. Desynchronization of cells on the developmental path triggers the formation of spiral waves of cAMP during Dictyostelium aggregation. Proc. Natl. Acad. Sci. U. S. A. 94, 9153–9158 (1997).
27 Grace, M. & Hütt, M.-T. Regulation of Spatiotemporal Patterns by Biological Variability: General Principles and Applications to Dictyostelium discoideum. PLOS Comput. Biol. 11, e1004367 (2015).
28 Odaka, H., Arai, S., Inoue, T. & Kitaguchi, T. Genetically-Encoded Yellow Fluorescent cAMP Indicator with an Expanded Dynamic Range for Dual-Color Imaging. PLoS One 9, e100252 (2014).
29 Fischer, M., Haase, I., Simmeth, E., Gerisch, G. & Müller-Taubenberger, A. A brilliant monomeric red fluorescent protein to visualize cytoskeleton dynamics in Dictyostelium. FEBS Lett. 577, 227–232 (2004).
30 Horikawa et al., submitted.
31 Lohmann, A. W., Dorsch, R. G., Mendlovic, D., Ferreira, C. & Zalevsky, Z. Space–bandwidth product of optical signals and systems. J. Opt. Soc. Am. A 13, 470 (1996).
32 Okamoto, K. et al. Single cell analysis reveals a biophysical aspect of collective cell-state transition in embryonic stem cell differentiation. Sci. Rep. 8, 1–13 (2018).
33 Watts, D. J. & Ashworth, J. M. Growth of myxameobae of the cellular slime mould Dictyostelium discoideum in axenic culture. Biochem. J. 119, 171–174 (1970).

Figures and Legends

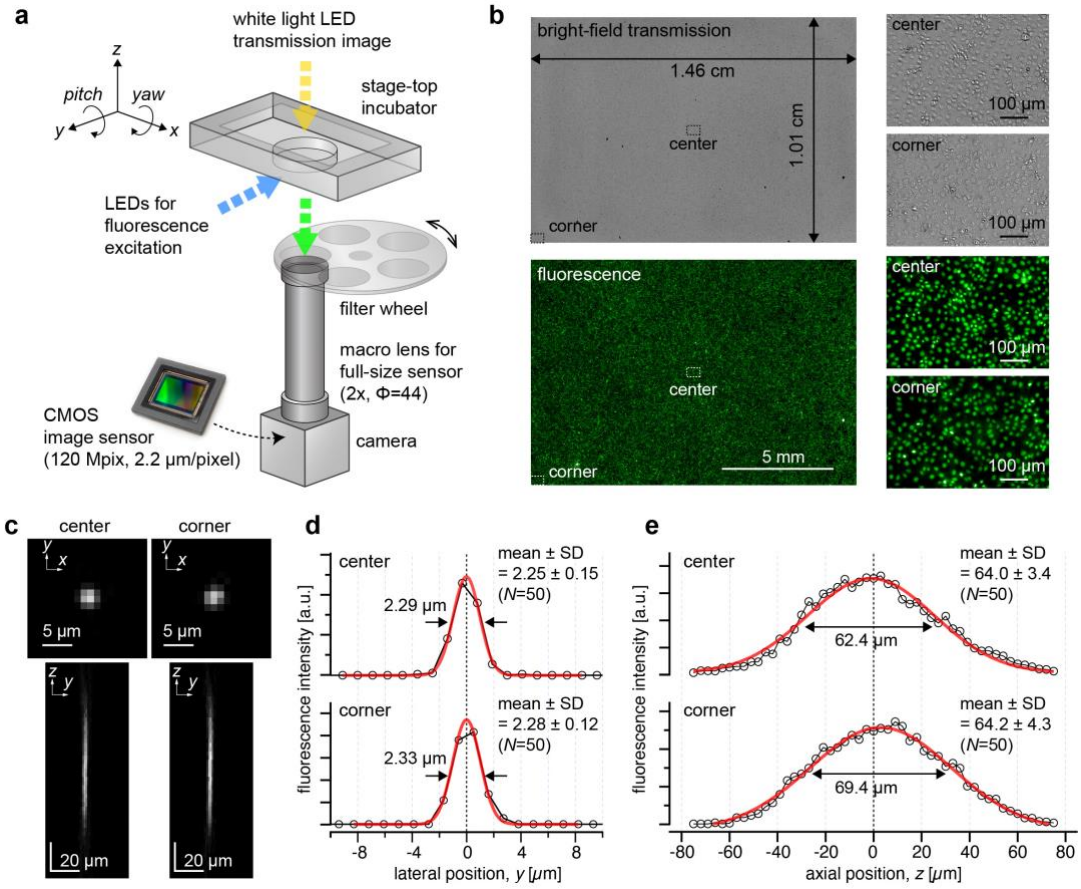

Figure 1: Configuration and performance of our trans-scale imaging system. (a) Schematic configuration of the system. (b) An example of trans-scale imaging of cells. Fluorescence imaging of cultured epithelial cells, fixed with paraformaldehyde and stained with NucleoSeeing, was performed with the 470 nm LED for excitation. (c-e) Evaluation of the imaging performance with beads with a diameter of 200 nm dispersed on a glass-bottom dish. Central wavelength of excitation light was 470 nm, and the emission peak wavelength was 520 nm. (c) Representative images in a transverse plane (*xy* plane) and a longitudinal plane (*yz* plane) at the center and corner of the FOV. (d) A line profile on the *y* axis in (c, top), shown with black circles. (d) A line profile on the *z* axis in (c, bottom), shown with black circles. The red lines in (d-e) represent a Gauss function curve fit to the experimental data.

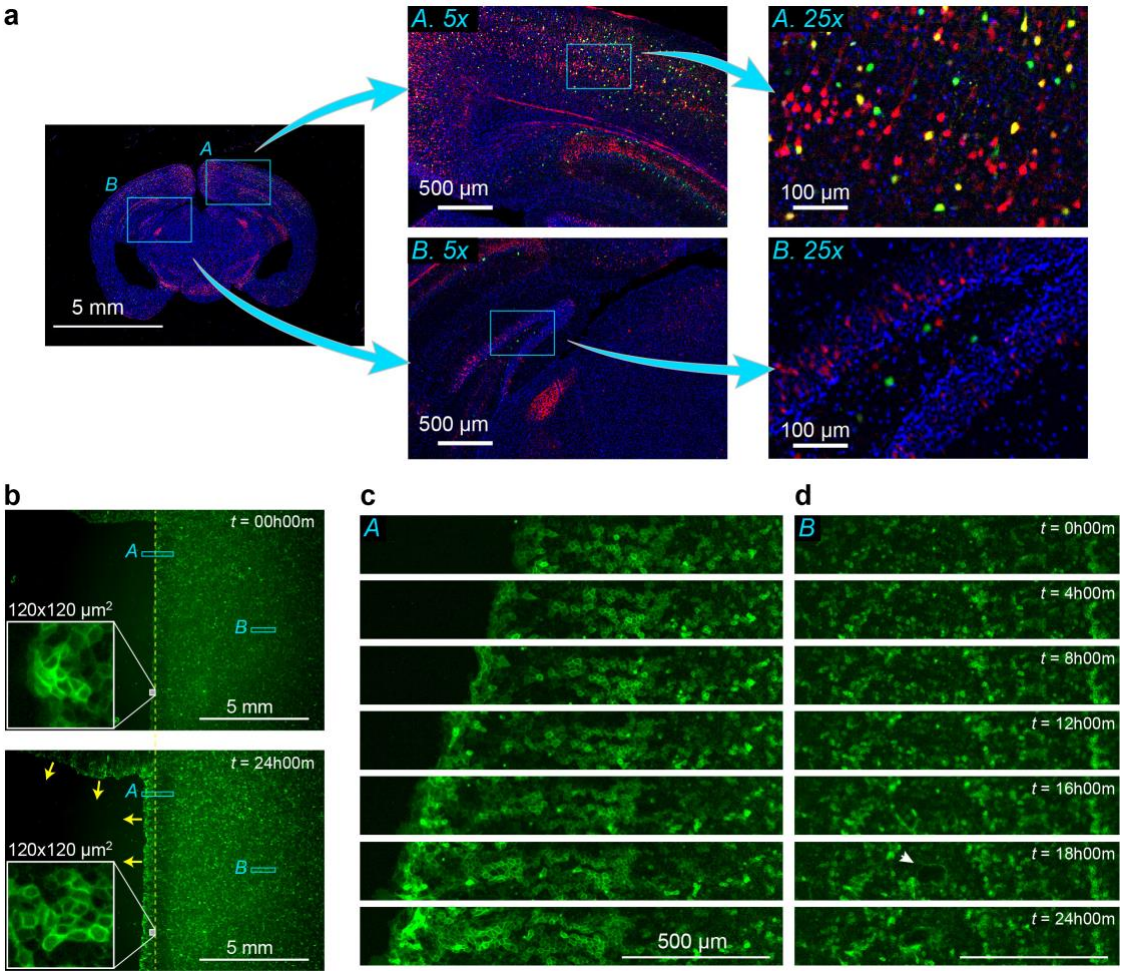

Figure 2: (a) Multi-color image of a mouse brain slice. Two regions of light-blue squares, cerebral cortex (*A*) and hippocampus (*B*), in the whole brain image (left) are magnified by 5-fold (middle). The local regions of light-blue squares in the 5x images are further magnified by 5-fold (right). Red, green, and blue represents the fluorescence intensity from tdTomato expressed on excitatory projection neurons, EGFP expressed on inhibitory interneurons, and Hoechst 33342 attached on nuclear DNA, respectively. (b-d) Time-lapse fluorescence imaging of collective cell migration in the wound healing in a cultured MDCK cells. The fluorescence images were acquired in 24 hours with 10 minutes interval. (b) The first and last frames of the full FOV. The closeup of the edge of the migration where individual cells can be recognized. (c-d) Seven frames in the magnified views indicated by the light-blue square regions *A* (c) and *B* (d) in the full FOV (b). The time intervals between frames is 4 hours.

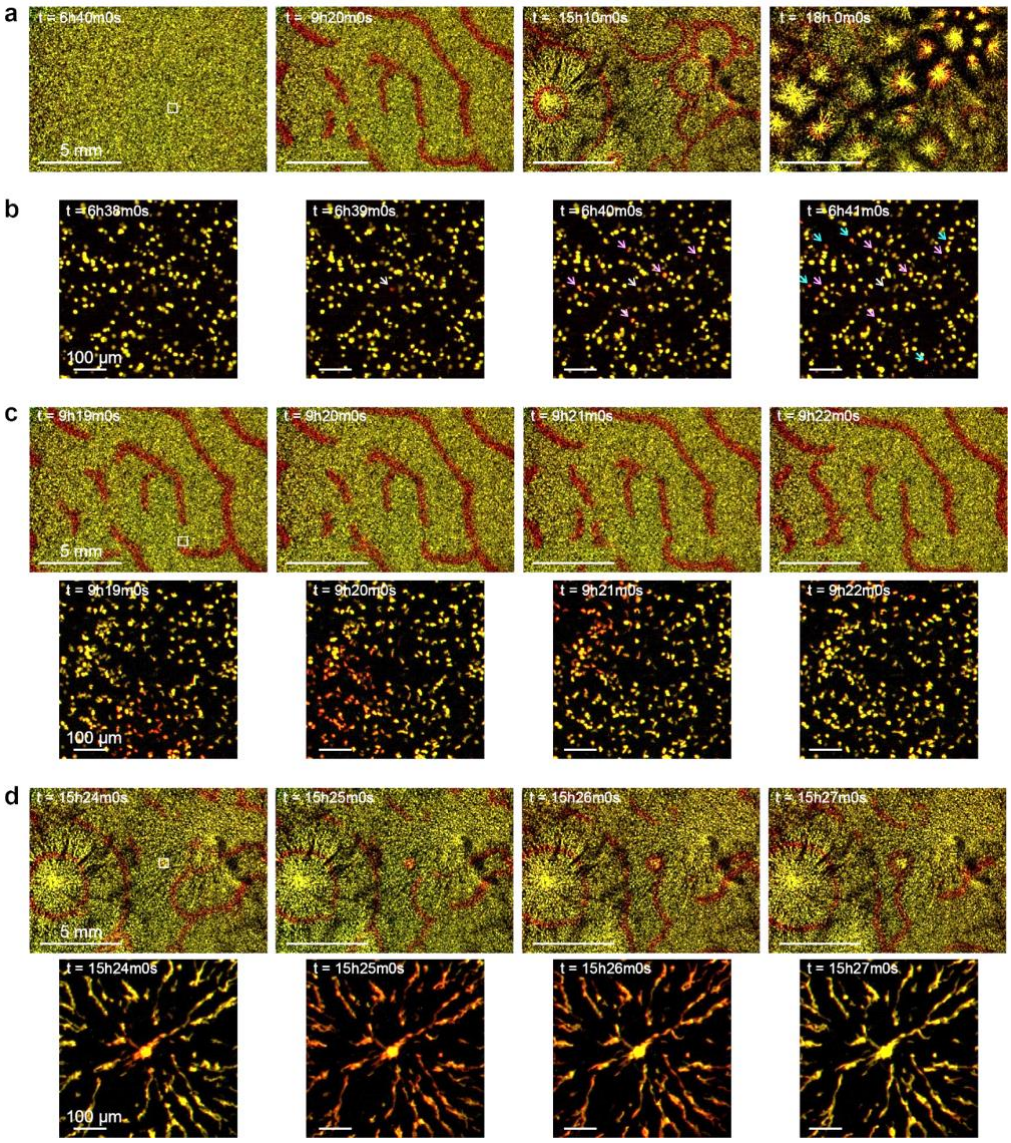

Figure 3: Spatial pattern formation of *D. discoideum* in centimeter scale. The *D. discoideum* cell expressing two fluorescent proteins, Flamindo2 and RFP, which are sensitive and insensitive to cAMP concentration, respectively. The images are exhibited in 8bit-RGB image, where the green and red colors reflect the intensity of Flamindo2 and RFP, respectively. The color scales are adjusted so that the cell color changes from yellow to red when cAMP concentration changes from low to high. The time counters indicate the time passed since starvation ($t = 0$). (a) Phase evolution of macroscopic pattern in the large time scale. (b) Emergence of leader and follower cells around t = 6h40m0s, shown in the magnified view of the square region in the left panel of (a). The leader cell is pointed with a white arrow, the follower cells are pointed with pink and light-blue arrows. (c) Propagation of spiral wave around t = 9h20m0s in the full FOV (top) and magnified view (bottom) of the square region in the top left panel. (d) Target wave propagation along with cell migration towards the center around t = 15h25m0s in the full FOV (top) and magnified view (bottom) of the square region in the top left panel.

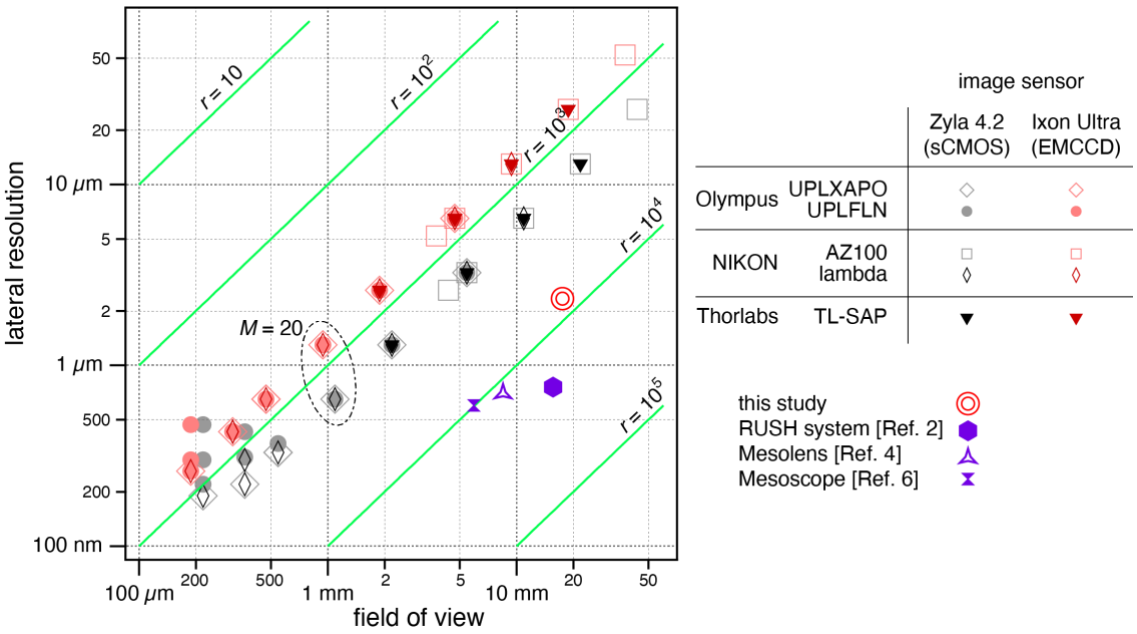

Figure 4: Comparative plots of FOV and lateral resolution of imaging systems composed of conventional microscope objectives and image sensors. Two series of Olympus, two series of NIKON, and a series of Thorlabs were chosen as objective lens, and Zyla 4.2 of Oxford Instruments were chosen as image sensors. The contour lines of trans-scalability index is drawn with the green lines. The performance of this study (AMATERAS1.0) and three previously reported imaging systems (Refs. 2, 4, 6) are also plotted for comparison.